FIRST PRINCIPLES *AB INITIO* STUDY OF CO_2 ADSORPTION ON THE KAOLINITE (001) SURFACE

MAN-CHAO HE, JIAN ZHAO*, AND YANG LI

State Key Laboratory for Geomechanics and Deep Underground Engineering, China University of Mining and Technology, Beijing 100083, China

Abstract—The capture and storage of carbon dioxide (CO_2) have considerable potential for mitigating climate change. Adsorption is one of the most popular methods for the storage of CO_2. The adsorption of CO_2 molecules on the hydroxylated (001) surface of kaolinite was investigated using density-functional theory within the generalized gradient approximation and a supercell approach. The coverage dependence of the adsorption structures and energetics was studied systematically for a wide range of coverage, Θ [from 0.11 to 1.0 monolayers (ML)], and adsorption sites. The CO_2 was adsorbed on the two-fold bridge-x (see the text for a definition) and the one-fold top-x sites in the bent, recumbent configuration, and on the three-fold hollow-z, two-fold bridge-z site, and the one-fold top-z sites in the vertical configuration. The surface-adsorbed binding site of CO_2 was strongest at the bridge-x site and weakest at the top-z site. The adsorption energy increased with coverage, thus indicating the greater stability of surface adsorption and a tendency to form CO_2 islands (clusters) with increasing coverage. The other properties of the CO_2/kaolinite (001) system, including the different charge distribution, the lattice relaxation, and the electronic density of states, were also studied and are discussed in detail.

 Key Words—Adsorption, Carbon Dioxide, First-principles Calculations, Kaolinite.

INTRODUCTION

The control of greenhouse gases is arguably the most challenging environmental policy issue facing the world today. Carbon dioxide is considered to be the major greenhouse gas (GHG) (He *et al*., 2012). The average concentration of CO_2 in the atmosphere has increased significantly from 280 ppm (parts per million) in about 1850 to 379 ppm in 2005 and as a result, the average global temperature has increased by $0.6-1$ºC during this period (Li *et al.*, 2013). The technology of CO_2 capture and storage (CCS) can provide a medium-term solution to mitigate environmental impacts (Kaya, 1995; Li *et al.*, 2013; Luis *et al.*, 2012; Aspelund and Jordal, 2007; Waldo, 2011). The technology of CCS usually consists of three parts: CO_2 capture, transport, and storage. Capture and storage have, by far, been the two most studied parts of the CCS chain, because transport has been considered to be the least technically challenging. As a result, many investigators have studied experimentally the storage of CO_2 using chemical and physical treatments. Adsorption is one of the most popular methods for the storage of CO_2 (Araki *et al.*, 2012; Lopez-Carreno *et al.*, 1997; Choe *et al.*, 2001; Do and Do, 2006; Baltrusaitis *et al.*, 2011; Smykowski *et al.*, 2013; Wood *et al.*, 2012). Natural clay minerals, in particular, have received much attention as a possible low-cost adsorbent in the storage of CO_2 taken from

contaminated air. A number of studies concerning clay minerals used to store CO_2 have been reported (Volzone, 2007; Venaruzzo *et al.*, 2002; Xu *et al.*, 2005; Ketzer *et al.*, 2009). Due to the limitations of the experimental methods used, a theoretical analysis of the adsorption mechanism of CO_2 monomers on natural clay minerals from a microscopic point of view will improve understanding of the adsorptive properties of the clay mineral−CO_2 interface and the influence of CO_2 adsorbed on the structure of clay minerals. Computer simulation based on density-functional theory (DFT) has proven a powerful and reliable tool in the study of CO_2−solid interfaces at the molecular level. Kaolinite is one of the most abundant clay minerals and so a greater insight into the adsorption of CO_2 molecules on kaolinite surfaces through detailed first-principles analysis is needed.

Existing experimental (Adams, 1983; Benco *et al.*, 2001; Bish, 1993) and theoretical (Hayashi, 1997; Hess and Saunders, 1992; Hobbs *et al.*, 1997; Plançon and Giese, 1997; Teppen, *et al.*, 1997; Hu and Angelos, 2008) data for the kaolinite $Al_2Si_2O_5(OH)_4$ surface are often rationalized by modeling two surfaces as almost perfect 1:1 layer structures consisting of two different aluminosilicate surfaces. One side consists of a gibbsite-type sheet where Al ions are coordinated octahedrally by oxygen ions and hydroxyl groups; the other side of the layer consists of a silica sheet in which Si ions are coordinated tetrahedrally by oxygen ions only. Quantitative estimates indicate that gibbsite-sheet OH groups and adjoining silica-sheet O atoms in kaolinite have a certain degree of van der Waals attraction and hydrogen bonding (Sato *et al.*, 2005). While the silica-

* E-mail address of corresponding author:
zhaojian0209@aliyun.com

sheet side is saturated and hydrophobic, the hydroxyl at the Al (oxyhydr)oxide side is hydrophilic. Kaolinite microparticles exist as hexagonal plates with a dominant (001) basal surface with almost perfect cleavage; this is the plane mainly exposed in kaolinite crystals (Šolc *et al.*, 2011; Giese, 1973). The kaolinite (001) hydroxyl surface is of primary interest in adsorption studies. The objectives here were to investigate CO_2 adsorption sites, adsorption energies, charge transfer, CO_2 structure during adsorption, and the structure of the intermediate reaction complex.

METHODS

Calculations were performed using the local-density approximation (LDA) as implemented in the Vienna *ab initio* simulation package (VASP) (Kress and Furthmüller, 1996). Projector augmented wave (PAW) pseudopotentials (Blöchl, 1994; Kress and Joubert, 1999) and plane waves were used. The energy cutoff for the plane-wave basis was 400 eV, which was sufficient to ensure errors of <0.01 eV in the calculated values for adsorption energies and activation barriers. The so-called 'repeated slab' geometries were applied. The kaolinite (001) surface was modeled using a slab composed of six atomic layers and a vacuum region of 20 Å, which was found to be sufficiently convergent. During the calculations, all the H, O, and Al atoms in the outermost three layers (octahedral Al oxide surface), as well as the CO_2 molecules, were allowed to relax while the other three atomic layers (including the middle O and H atoms, the bottom silica, and the O atoms) of the slab were kept fixed at the calculated bulk positions. Unless otherwise mentioned, a $(3 \times 3 \times 1)$ *k*-point grid

for the *p* (2×2) and *p* (3×3) surface cell with a Monkhorst-Pack (Monkhorst and Pack, 1976) scheme was used. A Fermi broadening of 0.02 eV/Å was chosen to smear the occupation of the bands around E_F by a finite-*T* Fermi function and extrapolating to $T = 0$ K. In the present study, calculations for adsorbed CO_2 molecules at surface coverages that ranged from 0.11 to 1.0 ML were performed for 12 adsorption sites (Figure 1). The 12 adsorption sites included three one-fold top sites (T_1-T_3), three two-fold bridge sites (B_1-B_3), and six three-fold hollow sites (H_1-H_6). The CO_2 coverages of 0.11, 0.33, 0.44, 0.67, 0.89, and 1.0 ML were calculated using the *p* (3×3) surface unit cell, while coverages of 0.25, 0.5, and 0.75 ML were calculated for the *p* (2×2) surface cell. The calculated lattice parameters of bulk kaolinite $a = 5.155$ Å, $b = 5.155$ Å, $c = 7.405$ Å, $\alpha = 75.14^o$, $\beta = 84.12^o$, and $\gamma = 60.18^o$ were used throughout the study (Hess and Saunders, 1992).

RESULTS

One important quantity, E_{ads}, tailored for the present study, is the average adsorption energy of the CO_2 molecules on the kaolinite substrate, defined as:

$$E_{ads}(\Theta) = -\frac{1}{N_{CO_2}} \left[E_{CO_2/kaolinite(001)} - E_{kaolinite(001)} - N_{CO_2} E_{CO_2} \right] \quad (1)$$
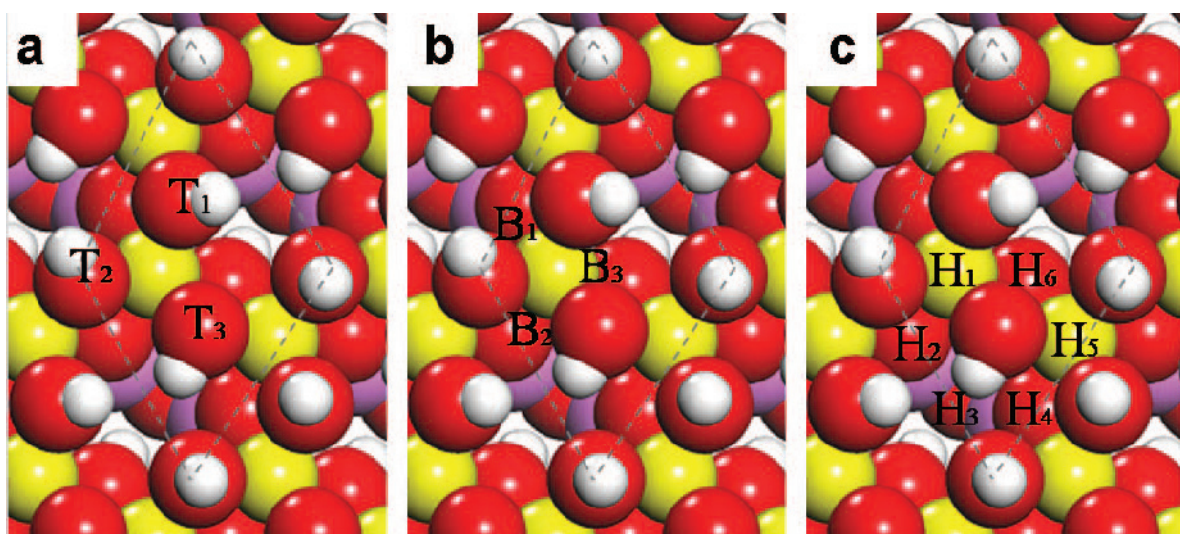
Here N_{CO_2} is the total number of CO_2 molecules present in the supercell at the coverage Θ considered (Θ is defined as the ratio of the number of molecules

Figure 1. Top view of the kaolinite (001) surface with (a) three top adsorption sites (T_1-T_3), (b) three bridge adsorption sites (B_1-B_3), and (c) six hollow adsorption sites (H_1-H_6). White spheres = hydrogen; red spheres = oxygen; yellow spheres = aluminum; and purple spheres = silicon.

adsorbed to the number of molecules in an ideal substrate layer). The $E_{CO_2/kaolinite\ (001)}$, $E_{kaolinite\ (001)}$, and E_{CO_2} are the total energies of the slabs containing CO$_2$, of the corresponding clean kaolinite surface, and of a free CO$_2$ molecule, respectively. According to this definition, a positive value of E_{ads} indicates that the adsorption is exothermic (stable) with respect to a free CO$_2$ molecule and a negative value indicates an endothermic (unstable) reaction. The adsorbed CO$_2$ coverage was $0 < \Theta \leqslant 1.0$. All of the three kinds of high-symmetry adsorption sites on the (001) surface were considered (Hu and Angelos, 2008). The x, y, and z were used to differentiate O−C−O orientations. As shown in Figure 1, 36 kinds of adsorption sites for CO$_2$ molecules on the kaolinite (001) surface were considered. By employing the notation used in Figure 1, the

sites as top1 (top2, top3)-x, y, z, bridge1 (bridge2, bridge3)-x, y, z, and hollow1 (hollow2, hollow3, hollow4, hollow5, hollow6)-x, y, z were represented. For optimization, the three kinds of top-x and bridge-x adsorption states with the CO$_2$ molecule recumbent (laying) on the surface were stable (Figure 2a,c). The recumbent orientation represented a configuration with one C and two O atoms of CO$_2$ forming bonds with the surface. The end-down orientation represented a configuration in which one oxygen atom of CO$_2$ formed a bond with the surface (Figure 2b,d,e). The adsorption sites of the end-down configuration were all of the three kinds of the top-z, bridge-z, and six kinds of hollow-z sites after geometry optimization, respectively. The O−C−O bond of adsorbed CO$_2$ molecules on all six kinds of hollow-z site had an angle with the kaolinite (001) surface.
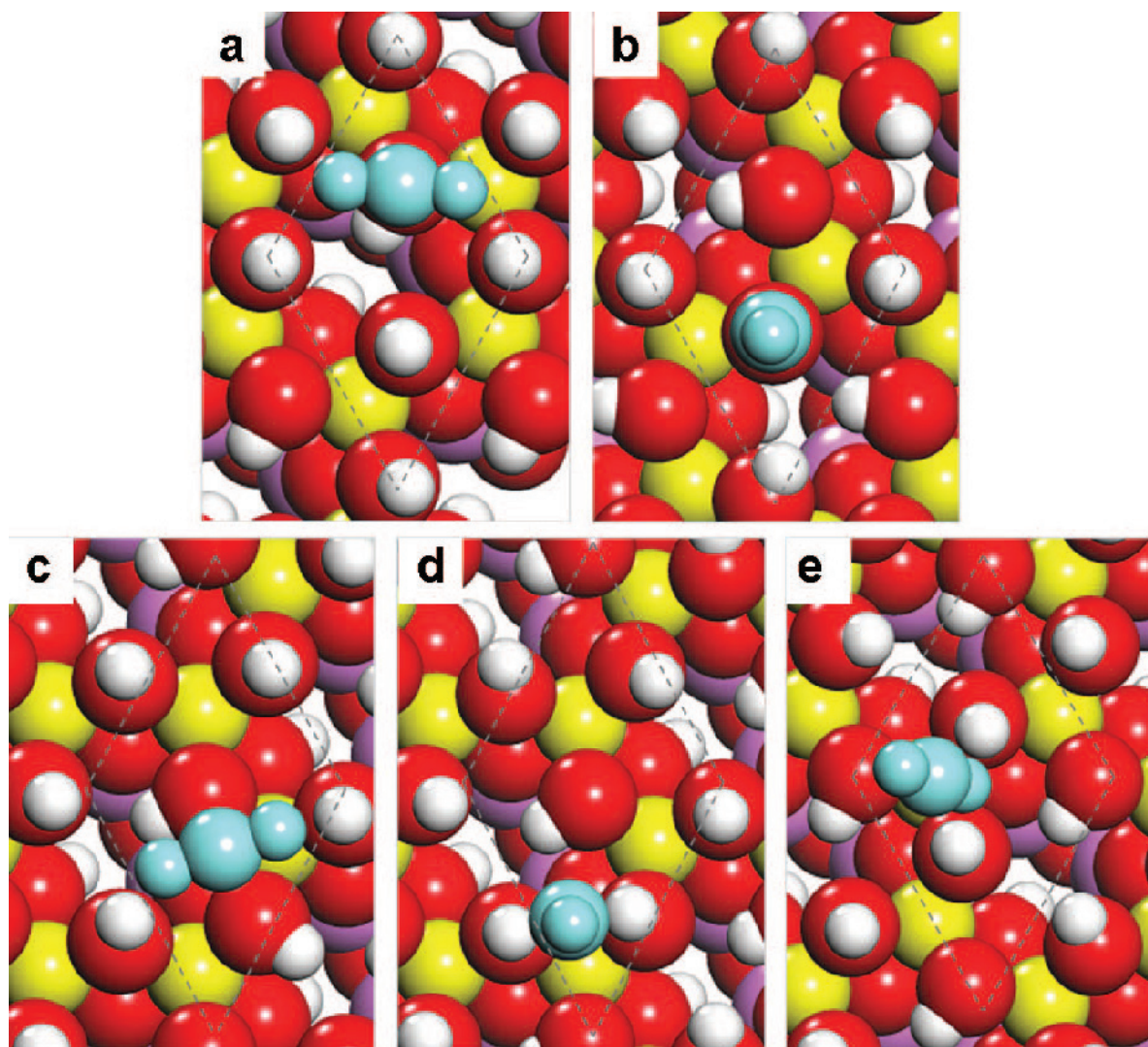

Figure 2. Top view of CO$_2$ molecule adsorbed on the (a) top-x, (b) top-z, (c) bridge-x, (d) bridge-z, and (e) hollow-z sites of kaolinite (001). The adsorbed CO$_2$ molecule is shown in blue for clarity.
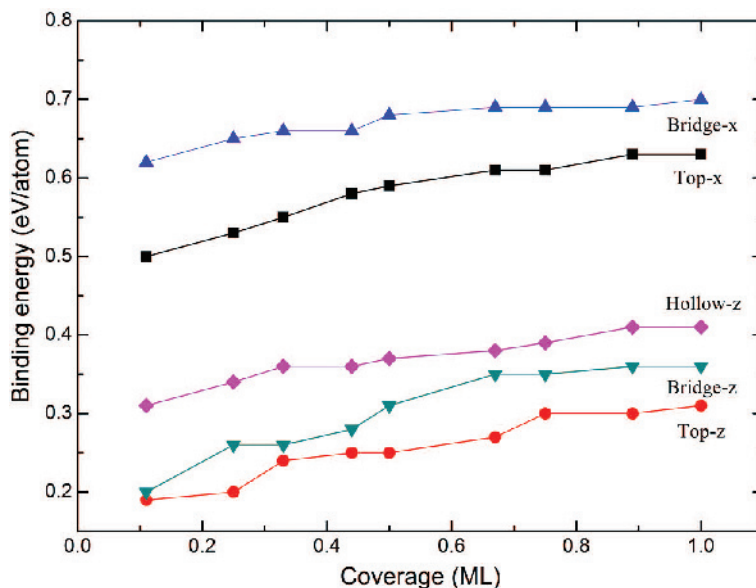
Figure 3. Calculated adsorption energy, E_{ads}, of the CO_2/kaolinite (001) system *vs.* the coverage for the CO_2 molecule adsorption in different sites. The solid lines connecting the calculated adsorption energies are used as visual guides.

Meanwhile, all three kinds of top-x, bridge-x, top-z, bridge-z, and six kinds of hollow-z adsorption sites for CO_2 molecules had similar adsorption energies in the coverage regime $0<\Theta \leqslant 1.0$. The calculated adsorption energies, E_{ads}, of CO_2 on these five kinds of surface sites with respect to the free molecule CO_2 are illustrated (Figure 3) and summarized (Table 1) for different CO_2 coverage in the regime $0<\Theta \leqslant 1.0$. The calculated adsorption energies (Figure 3) revealed that the x orientation adsorption was always greater than for the z orientation adsorption. For the x orientation adsorption, the bridge-x site was more stable than the top-x site while for the z orientation adsorption, the hollow-z was more favorable than the bridge-z and top-z sites in the coverage regime $0<\Theta \leqslant 1.0$. Meanwhile, the quantity for top-x, top-z, bridge-x, bridge-z, and hollow-z adsorption displayed a modestly increasing tendency with the CO_2 coverage (Figure 3), while the overall variation in the magnitude of E_{ads} was rather small in the range of coverage. The increasing adsorption with coverage indicated a significant attraction between the on-surface CO_2 molecules and implied a tendency to form CO_2 islands or clusters on the kaolinite (001) surface at $0<\Theta \leqslant 1.0$. In addition, the adsorption-energy difference between the top-x and bridge-x sites, as well as among the top-z, bridge-z, and hollow-z, displayed a notable increase with CO_2 coverage, which implied a substrate-induced anisotropy in the CO_2−solid chemical bonding.

Calculated geometries for CO_2-molecule adsorption on top-x, top-z, bridge-x, bridge-z, and hollow-z sites of kaolinite (001) at $\Theta = 0.25, 0.5, 0.75,$ and 1.0, including the C−O bond lengths, d_{C-O} (Å), and bond angles, $\angle OCO$ (°), are listed in Table 2. In the first row of that table, the calculated values for a gaseous CO_2 molecule are listed for comparison. For all the adsorption sites, the two C−O bond lengths, d_{C-O1} and d_{C-O2}, varied little around 1.17 Å with increasing Θ values. The values of the O−C−O internal angle ($\angle OCO$) for all five types of adsorption sites decreased with increasing Θ. Compared with the gas-phase value, $\angle OCO$ on the top-z and bridge-z sites decreased by 11° and 7° from 180°, respectively, while on the top-x, bridge-x, and hollow-z, $\angle OCO$ varied little around 180°. For different CO_2 coverage values, Θ, the height, h_{CO_2-H}, of adsorbate CO_2 above the surface

Table 1. The calculated adsorption energy, E_{ads} (eV), as a function of molecular CO_2 coverage on the different sites of kaolinite (001).

Site	ML0.11	ML0.25	ML0.33	ML0.44	ML0.5	ML0.67	ML0.75	ML0.89	ML1.0
Top-x	0.50	0.53	0.55	0.58	0.59	0.61	0.61	0.63	0.63
Top-z	0.19	0.20	0.24	0.25	0.25	0.27	0.30	0.30	0.31
Bridge-x	0.62	0.65	0.66	0.66	0.68	0.69	0.69	0.69	0.70
Bridge-z	0.20	0.26	0.26	0.28	0.31	0.35	0.35	0.36	0.36
Hollow-z	0.31	0.34	0.36	0.36	0.37	0.38	0.39	0.41	0.41

Table 2. The calculated geometries for the CO$_2$ molecule adsorption on top-x, top-z, bridge-x, bridge-z, and hollow-z sites of kaolinite (001). The C−O bond lengths d_{C-O} (Å) and bond angles (∠OCO) (º) of CO$_2$ molecules are listed. The first row lists the calculated values for a gaseous CO$_2$ molecule for comparison.

Site	d_{C-O1} (Å)				d_{C-O2} (Å)				∠OCO			
	Ml0.25	Ml0.5	Ml0.75	Ml1.0	Ml0.25	Ml0.5	Ml0.75	Ml1.0	Ml0.25	Ml0.5	Ml0.75	Ml1.0
Free	1.16	1.16	1.16	1.16	1.16	1.16	1.16	1.16	180.0	180.0	180.0	180.0
Top-x	1.17	1.17	1.17	1.17	1.16	1.16	1.16	1.16	179.9	179.7	179.7	179.5
Top-z	1.18	1.18	1.18	1.17	1.18	1.18	1.17	1.17	169.1	168.1	168.0	171.2
Bridge-x	1.17	1.17	1.17	1.17	1.16	1.16	1.16	1.16	179.9	179.7	179.9	179.3
Bridge-z	1.17	1. 17	1.17	1.17	1.17	1.17	1.17	1.17	172.5	171.9	171.9	172.1
Hollow-z	1.17	1.17	1.17	1.17	1.17	1.16	1.16	1.16	179.9	179.6	179.2	179.2

and the topmost interlayer relaxation Δd_{12} with CO$_2$ in the top-x, bridge-x, top-z, bridge-z, and hollow-z sites are summarized in Table 3. The Δd_{12} value was calculated according to the equation $\Delta d_{12} = (d_{12}-d_0)/d_0$, where d_{12} and d_0 were the depth between the first and second layers of the relaxed surface and the corresponding depth between the first and second layers of the clean kaolinite (001) surface, respectively. The calculated results showed that the adsorption of CO$_2$ on kaolinite (001) induced notable changes in the interlayer distance of the substrate. In particular, for the top-x, top-z, bridge-z, and hollow-z adsorption, the value of Δd_{12} was negative and decreased with CO$_2$ coverage, which meant that the distance between the topmost two atomic layers of the kaolinite (001) surface had contracted with increasing CO$_2$ coverage. On the contrary, for bridge-x adsorption, the value of Δd_{12} was negative from −7.63% to −14.06% in the coverage regime $0.11 \leqslant \Theta \leqslant 1.0$, which meant the topmost interlayer had also contracted but became smaller with increasing CO$_2$ coverage. These changes reflected the strong influence of the CO$_2$ adsorbates on the neighboring O atoms and, thus, resulted from significant redistribution of the electronic structure. The results verified that CO$_2$ adsorption caused the outermost kaolinite (001) layer separation to relax back to something close to its 'ideal' bulk value. With respect to the height h_{CO_2-H} of adsorbate CO$_2$ above the surface, the results showed (Table 3) that, for all five types of adsorption sites, the values of h_{CO_2-H} decreased with increasing Θ. The short height h_{CO_2-H}

implied a strong interaction between the CO$_2$ and kaolinite surfaces. Note that the bridge-x site was slightly shorter than the other four types of sites, consistent with the fact that the bridge-x site was the most stable.

To gain more insight into the precise nature of the chemisorbed molecular state in the CO$_2$/kaolinite (001) system, the electronic partial density of state (PDOS) of the CO$_2$ molecule and the neighboring O atoms were calculated. The results were analyzed by means of the electron density difference $\Delta\rho(r)$ which was obtained by subtracting the electron densities of non-interacting component systems, $\rho^{kaolinite\ (001)}(r) + \rho CO_2(r)$, from the density $\rho(r)$ of the CO$_2$/kaolinite (001) system, while retaining the atomic positions of the component system at the same location as in CO$_2$/kaolinite (001). Positive (blue) $\rho(r)$ indicated an accumulation of electron density upon binding, while a negative (yellow) corresponded to electron-density depletion. As a typical example, the PDOS for the two kinds of stable adsorption configuration of top-z and bridge-x were plotted (Figure 4); the electron-density differences are shown in Figure 4b,f (insets). For comparison, the PDOS of the free CO$_2$ molecule and the neighboring O atoms of clean kaolinite (001) were also calculated. After CO$_2$-molecule adsorption on the top-z site of kaolinite (001), the 3σ, 4σ, 1π, 5σ bonding, and 2π antibonding orbitals of CO$_2$ shifted down in energy by 3.70, 3.53, 3.85, 3.55, and 3.85 eV, respectively. Furthermore, the amplitudes of all bonding and antibonding orbitals were much weaker than those in

Table 3. The calculated adsorbate height (h_{C-O}) and the interlayer relaxation (Δd_{12}) for different coverage of atomic CO$_2$ adsorption on the kaolinite (001) surface.

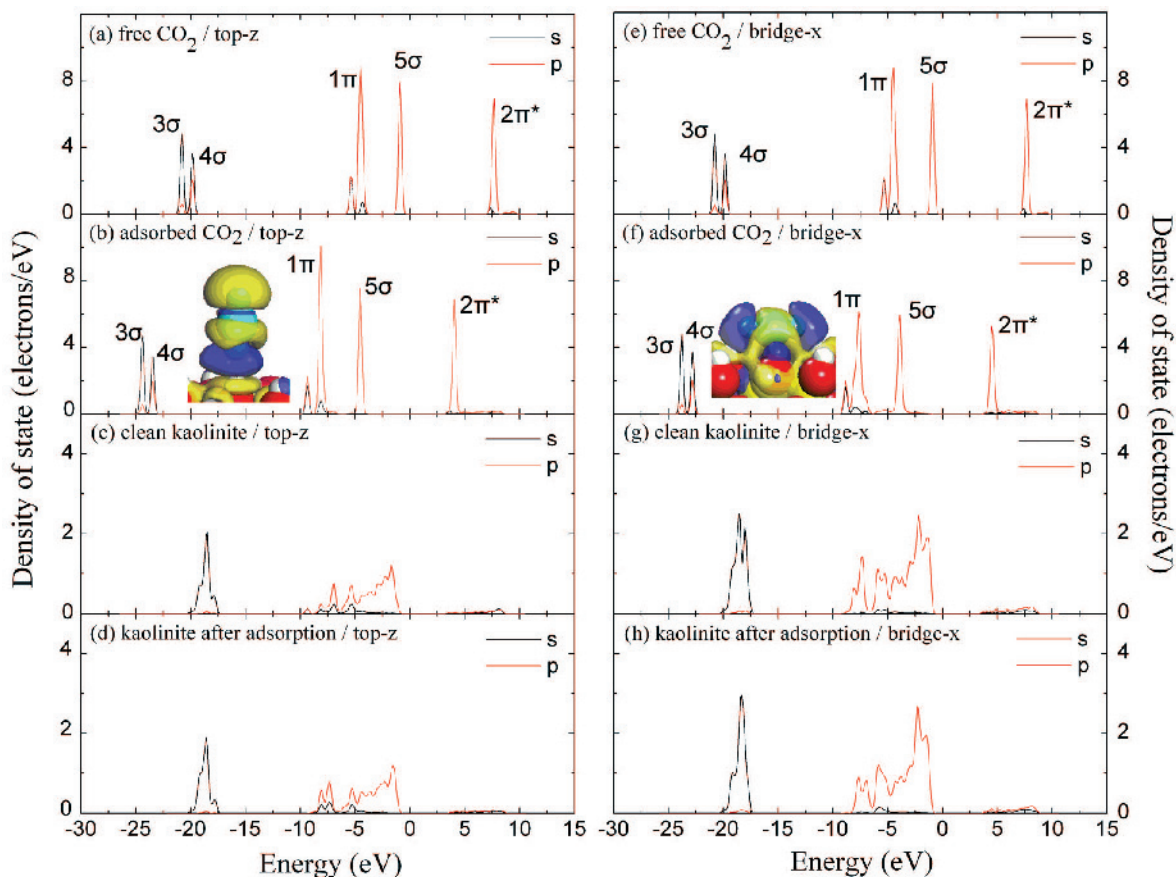| Coverage Θ	h_{C-O}				Δd_{12} (%)			
	0.25 ML	0.5 ML	0.75 ML	1.0 ML	0.25 ML	0.5 ML	0.75 ML	1.0 ML
Top-x	2.13	2.13	2.08	2.03	−6.01	−5.38	−4.84	−4.63
Top-z	4.02	3.83	3.64	3.51	−7.77	−6.83	−6.53	−5.89
Bridge-x	2.29	2.27	2.27	2.26	−7.63	−10.62	−10.62	−14.06
Bridge-z	3.79	3.64	3.49	3.31	−7.13	−6.20	−5.19	−4.93
Hollow-z	3.78	3.49	3.26	3.12	−7.14	−6.34	−5.87	−5.64

Figure 4. The PDOS plots for the CO_2 molecule and the neighboring O atoms bonded to CO_2 at the stable top-z and bridge-x adsorption sites on surface: (a,b) free and adsorbed CO_2 molecule at the stable top-z adsorption site; (c,d) clean and adsorbed kaolinite (001) surface at the stable top-z adsorption site; (e,f) free and adsorbed CO_2 molecule at the stable bridge-x adsorption site; (g,h) clean and adsorbed kaolinite (001) surface at the stable bridge-x adsorption site. The insets show the side view of electron density difference for the CO_2 atom at the stable (b) top-z and (f) bridge-x adsorption sites. The Fermi energy is set at zero.

the free CO_2. These features were essentially caused by the different electronegativities of kaolinite and CO_2 molecules, which induced charge redistribution and thus built a global electrostatic attraction between the CO_2 and neighboring O atoms. The result was substantiated by the 3D electron density difference. A large charge accumulation existed between the adsorbate and substrate; an O−O bond was formed, which donated electrons from a neighboring surface O atom to the CO_2 molecule. The PDOS for the most stable adsorption configuration of bridge-x was calculated (Figure 4e,h). The bonding and antibonding orbitals of the CO_2 molecule were shifted to a much lower energy and the amplitudes of 1π bonding and 2π antibonding were weaker than those in free CO_2 molecules, even in the adsorbed CO_2 on the top-z site. The sp electronic states of adsorbed CO_2, in particular, expanded in energy compared with free CO_2 and the adsorbed CO_2 on the top-z site. The overlap in energy between adsorbed CO_2 and neighboring O atoms of kaolinite (001) surface electrons ranged from −9.15 eV to −3.46 eV. From the

3D electron-density difference (Figure 4h, inset), one C−O and two H−O bonds were formed, among which two donate electrons from surface H atoms to the O atoms of the CO_2 molecule and donated electrons from the C atom of the CO_2 molecule to neighboring surface O atoms. These results illustrated that the bridge-x adsorption site was more stable than the top-z adsorption site for CO_2 molecules.

The orbital-resolved PDOS for CO_2 adsorption on the bridge-x site, and the neighboring O and H atoms at $\Theta = 0.11$ and $\Theta = 1.0$, are shown in Figures 5a and 5b, respectively. The Fermi energy was set at zero. At low coverage ($\Theta = 0.11$), the narrow, low-amplitude peak at $\sim −7.92$ eV was denoted the 'CO_2 p state' (Figure 5a), which was largely hybridized with the p state of the neighboring O atoms; the hybridization between CO_2 p and O sp states was negligible. With increasing CO_2 coverage (Figure 5b for $\Theta = 1.0$ ML), three prominent changes involving the C−O chemical bonding occurred: (1) the peaks in the CO_2 3σ, 4σ, 1π, 5σ bonding, and 2π antibonding shifted down in energy; the amplitudes of all
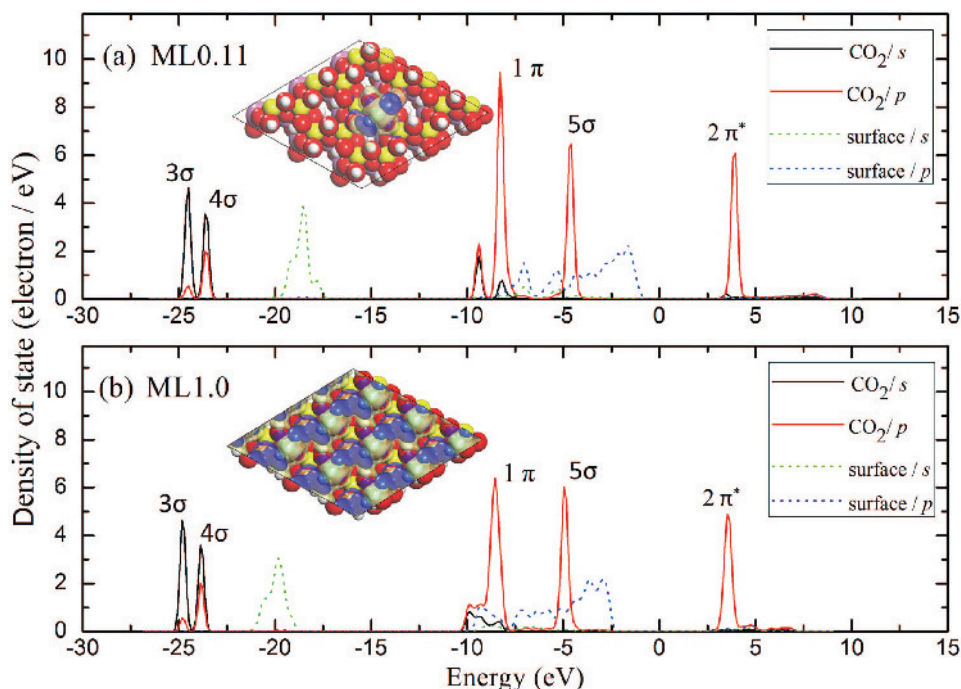
Figure 5. The PDOS for the bridge-x adsorption site on surface CO$_2$ molecules and the neighboring O atoms at (a) $\Theta = 0.11$ and (b) $\Theta = 1.0$ where the inset shows the top view of electron density difference for CO$_2$ atoms at $\Theta = 0.11$ and $\Theta = 1.0$, respectively. The Fermi energy is set at zero.

bonding and antibonding orbitals were much weaker than those in the case of $\Theta = 0.11$ ML. (2) Compared to the case where $\Theta = 0.11$ ML, the hybridization of CO$_2$ p and surface O p states was distinctly enhanced in the case of $\Theta = 1.0$ ML. The change in the CO$_2$ p PDOS was due to the fact that at high coverage for $\Theta = 1.0$ ML, the CO$_2$ adatom was highly coordinated, which drove the CO$_2$ p state to bond not only with the s states but also the p states of the O and H atoms. Because the O sp states lay mainly in the interior of the valence band, the CO$_2$ p state thus had to shift down in energy in order to overlap with the O p states. In particular, the main peak around $E = -8.6$ eV in the CO$_2$ p PDOS in Figure 5b was a result of the hybridization between CO$_2$ p states and O sp states. (3) The small CO$_2$ peak at -9.36 eV tended to vanish due to a large weight transfer of these states to a higher energy, caused by the formation of bonding states between CO$_2$ p and O p orbitals. This was most notable for surface O p states. In fact, in the $-9.7 < E < -7.9$ eV energy interval (Figure 5b), a large number of surface O p states were empty in this energy region at low CO$_2$ coverage (Figure 5a) of the kaolinite (001) surface. The empty O p states will gain energy, which will over-compensate the energy lost by elevation of the CO$_2$ p state when adsorbed CO$_2$ coverage is increased. A top view of the electron density difference between CO$_2$ atoms at $\Theta = 0.11$ and $\Theta = 1.0$ (Figures 5a and 5b) reveals that the charge redistribution was mainly at the surface and involved the adsorbed CO$_2$ molecule and the topmost O atoms. The results further revealed that upon adsorption,

electrons flowed from the O p state into the CO$_2$ p state, resulting in a depletion of the surface electrons. With increasing CO$_2$ coverage, more surface O sp electrons transferred to the localized CO$_2$ 1π and 5σ orbitals, suggesting that the covalent character of the O$-$O bonding increased with CO$_2$ coverage (Figure 5b, inset).

SUMMARY

The adsorption of CO$_2$ molecules on the kaolinite (001) surface were investigated systematically using first-principles DFT-LDA calculations. A wide range of coverage from 0.11 to 1.0 ML was considered using different surface models [*i.e.* p (3$\times$3) and p (2$\times$2) surface unit cells] for adsorption in the surface top-x, top-z, bridge-x, bridge-z, and hollow-z sites. In the coverage range of $0 < \Theta < 1.0$, the most stable among all possible pure adsorbed sites was the bridge-x site, followed by the top-x, hollow-z, bridge-z, and top-z sites. The atomic geometry, the charge-density distribution, and the electronic structure upon the adsorbed CO$_2$ was also studied, which showed consistently the fundamental influence of covalent bonding between the CO$_2$ molecule and surface O atoms. Remarkably, this influence on the energy increased with increasing the CO$_2$ coverage. The increase in the CO$_2$ adsorption energy for all five types of sites with Θ in the coverage range $0 < \Theta \leqslant 1.0$ implied the effective attraction between the CO$_2$ adsorbates and kaolinite (001) surface, making it favorable for the formation of CO$_2$ islands or clusters.

REFERENCES

Adams, J.M. (1983) Hydrogen atom position in kaolinite by neutron profile refinement. *Clays and Clay Minerals*, **31**, 352–358.

Araki, S., Kiyohara, Y., Tanaka, S., and Miyake, Y. (2012) Adsorption of carbon dioxide and nitrogen on zeolite rho prepared by hydrothermal synthesis using 18-crown-6 ether. *Journal of Colloid and Interface Science*, **388**, 185–190.

Aspelund, A. and Jordal, K. (2007) Gas conditioning − the interface between CO_2 capture and transport. *Greenhouse Gas Control I*, 343–354.

Baltrusaitis, J., Schuttlefield, J., Zeitler, E., and Grassian, V.H. (2011) Carbon dioxide adsorption on oxide nanoparticle surface. *Chemical Engineering Journal*, **170**, 471–481.

Benco, L., Tunega, D., Hafner, J., and Lischka, H. (2001) Orientation of OH groups in kaolinite and dickite: *ab initio* molecular dynamics study. *American Mineralogist*, **86**, 1057–1065.

Bish, D.L. (1993) Rietveld refinement of the kaolinite structure at 1.5 K. *Clays and Clay Minerals*, **41**, 738–744.

Blöchl, P.E. (1994) Projector augmented-wave method. *Physical Review B*, **50**, 17953–17979.

Choe, S.J., Kang, H.J., Park, D.H., Huh, D.S., and Park, J. (2001) Adsorption and dissociation reaction of carbon dioxide on Ni(111) surface: Molecular orbital study. *Applied Surface Science*, **181**, 265–276.

Do, D.D. and Do, H.D. (2006) Effects of potential models on the adsorption of carbon dioxide on graphitized thermal carbon black: GCMC computer simulations. *Colloids and Surface A*, **277**, 239–248.

Giese, R.F., JR. (1973) Interlayer bonding in kaolinite dickite and nacrite. *Clays and Clay Minerals*, **21**, 145–149.

Hayashi, S. (1997) NMR study of dynamics and evolution of guest molecules in kaolinite/dimethyl sulfoxide intercalation compound. *Clays and Clay Minerals*, **45**, 724–732.

He, M.C., Sousa, L.R., Elsworth, D., and Vargas, E. Jr., editors (2012) *CO_2 Storage in Carboniferous Formations and Abandoned Coal Mines*. CRC Press, Oxford, UK, pp. 1–68.

Hess, A.C. and Saunders, V.R. (1992) Periodic ab initio Hartree-Fock calculation of the low-symmetry mineral kaolinite. *The Journal of Physical Chemistry*, **11**, 4367–4374.

Hobbs, J.D., Cygan, R.T., Nagy, K.L., Schultz, P.A., and Sears, M.P. (1997) All-atom *ab initio* energy minimization of the kaolinite crystal structure. *American Mineralogist*, **82**, 657–662.

Hu, X.L. and Angelos, M. (2008) Water on the hydroxylated (001) surface of kaolinite: From monomer adsorption to a flat 2D wetting layer. *Surface Science*, **602**, 960–974.

Kaya, Y. (1995) The role of CO_2 removal and disposal. *Energy Conversion and Management*, **6–9**, 375–380.

Ketzer, J.M., Iglesias, R., Einloft, S., Dullius, J., Ligabue, R., and Lima, V.D. (2009) Water-rock-CO_2 interactions in saline aquifers aimed for carbon dioxide storage: Experimental and numerical modeling studies of the Rio Bonito Formation (Permian), southern Brazil. *Applied Geochemistry*, **24**, 760–767.

Kresse, G. and Furthmuller, J. (1996) Efficient iterative schemes for ab initio total-energy calculations using a plane-wave basis set. *Physical Review B*, **54**, 11169–11173.

Kresse, G. and Joubert, J. (1999) From ultrasoft pseudopotentials to the projector augmented-wave method. *Physical Review B*, **59**, 1758–1762.

Li, L., Zhao, N., Wei, W., and Sun, Y.H. (2013) A review of research progress on CO_2 capture, storage, and utilization in Chinese Academy of Sciences. *Fuel*, **108**, 112–130.

Lopez-Carreno, L.D., Heras, J.M., and Viscido, L. (1997) Adsorption and dissociation of CO_2 on polycrystalline Mo. *Surface Science*, **377–379**, 615–618.

Luis, P., Gerven, T.V., and Bruggen, B.V. (2012) Recent developments in membrane-based technologies for CO_2 capture. *Progress in Energy and Combustion Science*, **38**, 419–448.

Monkhorst, H.J. and Pack, J.D. (1976) Special points for Brillouin-zone integrations. *Physical Review B*, **13**, 5188–5192.

Plançon, A., Giese, R.F. Jr., Snyder, R., Drits, V.A., and Bookin, A.S. (1997) Stacking faults in the kaolinite-group minerals: defect structures of kaolinite. *Clays and Clay Minerals*, **37**, 195–198.

Sato, H., Ono, K., Johnston, C.T., and Yamagishi, A. (2005) First-principles studies on the elastic constants of a 1:1 layered kaolinite mineral. *American Mineralogist*, **90**, 1824–1826.

Smykowski, D., Szyja, B., and Szczygiel, J. (2013) DFT modeling of CO_2 adsorption on Cu, Zn, Ni, Pd/DOH Zeolite. *Journal of Molecular Graphics and Modelling*, **41**, 89–96.

Šolc, R., Gerzabek, M.H., Lischka, H., and Tunega, D. (2011) Wettability of kaolinite (001) surfaces − Molecular dynamics study. *Geoderma*, **169**, 47–54.

Teppen, B.J., Rasmussen, K., Bertsch, P.M., Miller, D.M., and Schäfer, L. (1997) Molecular dynamics modeling of clay minerals. 1. Gibbsite, kaolinite, pyrophyllite, and beidellite. *The Journal of Physical Chemistry B*, **101**, 1579–1587.

Venaruzzo, J.L., Volzone, C., Rueda, M.L., and Ortida, J. (2002) Modified bentonitic clay minerals as adsorbents of CO, CO_2, and SO_2 gases. *Microporous and Mesoporous Materials*, **56**, 73–80.

Volzone, C. (2007) Retention of pollutant gases: comparison between clay minerals and their modified products. *Applied Clay Science*, **36**, 191–196.

Waldo, P. (2011) Clay minerals, carbon storage, and effects of observational scale on computational models. *Applied Clay Science*, **78**, 4059–4062.

Wood, B.C., Bhide, S.Y., Dutta, D., Kandagal, V.S., Pathak, A.D., Punnathanam, S.N., Ayappa, K.G., and Narasimhan, S. (2012) Methane and carbon dioxide adsorption on edge functionalized graphene: A comparative DFT study. *The Journal of Chemical Physics*, **137**, 054702.

Xu, T.F., Apps, J.A., and Pruess, K. (2005) Mineral sequestration of carbon dioxide in a sandstone-shale system. *Chemical Geology*, **217**, 295–318.